Earth and Planetary Science Letters 302 (2011) 378–384

Contents lists available at ScienceDirect

Earth and Planetary Science Letters

journal homepage: www.elsevier.com/locate/epsl

$\delta^{13}C$ evidence that high primary productivity delayed recovery from end-Permian mass extinction

K.M. Meyer [a,*], M. Yu [b], A.B. Jost [a], B.M. Kelley [a], J.L. Payne [a]

[a] Department of Geological & Environmental Sciences, Stanford University, 450 Serra Mall, Building 320, Stanford, CA 94305, USA
[b] College of Resource and Environment Engineering, Guizhou University, Caijiaguan, Guiyang 550003, Guizhou Province, PR China

ARTICLE INFO

Article history:
Received 28 June 2010
Received in revised form 14 December 2010
Accepted 15 December 2010
Available online 13 January 2011

Editor: P. DeMenocal

Keywords:
Permian–Triassic boundary
extinction
biotic recovery
stable carbon isotopes
anoxia
euxinia

ABSTRACT

Euxinia was widespread during and after the end-Permian mass extinction and is commonly cited as an explanation for delayed biotic recovery during Early Triassic time. This anoxic, sulfidic episode has been ascribed to both low- and high-productivity states in the marine water column, leaving the causes of euxinia and the mechanisms underlying delayed recovery poorly understood. Here we use isotopic analysis to examine the changing chemical structure of the water column through the recovery interval and thereby better constrain paleoproductivity. The $\delta^{13}C$ of limestones from 5 stratigraphic sections in south China displays a negative gradient of approximately 4‰ from shallow-to-deep water facies within the Lower Triassic. This intense gradient declines within Spathian and lowermost Middle Triassic strata, coincident with accelerated biotic recovery and carbon cycle stabilization. Model simulations show that high nutrient levels and a vigorous biological pump are required to sustain such a large gradient in $\delta^{13}C$, indicating that Early Triassic ocean anoxia and delayed recovery of benthic animal ecosystems resulted from too much productivity rather than too little.

1. Introduction

Nearly nine in ten marine animal species were lost at the Permian–Triassic (P–T) boundary and terrestrial ecosystems were similarly devastated (Erwin, 2006). Recovery of benthic marine ecosystems was largely delayed for ~5 Ma until the end of the Early Triassic (Erwin, 2007; Hallam, 1991; Payne et al., 2004); the pace of recovery accelerated during the Middle Triassic, exemplified by the return of reef ecosystems and the first occurrence of modern reef-building corals (scleractinians) (Flugel, 2002). Extensive and persistent marine anoxia and euxinia are widely cited as the primary factor limiting recovery during Early Triassic time (Hallam, 1991; Isozaki, 1997; Wignall and Twitchett, 2002a,b). Middle Triassic diversification coincided with the waning of anoxia and stabilization of the global carbon cycle (Grice et al., 2005; Payne et al., 2004; Wignall and Twitchett, 2002a,b). However, the oceanographic mechanisms responsible for these phenomena remain poorly constrained.

Two contrasting scenarios could relate euxinia to the associated state of marine productivity during the Permian and Triassic. Climate warming at the end of the Permian could have reduced rates of physical circulation, leading to oceanic anoxia and to a collapse of the biological pump (Rampino and Caldeira, 2005). The ensuing low-productivity ocean (Twitchett, 2006; Twitchett et al., 2001) could have delayed the recovery of marine animal ecosystems through inadequate food resources (Twitchett et al., 2001) and habitat restriction from shallow-marine anoxia (Wignall and Twitchett, 2002a). Alternatively, high levels of primary production in the surface ocean could have sustained anoxic and sulfidic conditions and thereby repressed the recovery of marine animal communities through habitat restriction from anoxia and, potentially, domination of primary productivity by bacteria with low nutrient value to animal consumers (Hotinski et al., 2001; Meyer et al., 2008; Payne and Finnegan, 2006; Payne and van de Schootbrugge, 2007; Xie et al., 2005).

Both the low- and high-productivity scenarios can account for many aspects of the P–T biological and geochemical records, but the substantial marine biogeochemical differences between these hypotheses imply contrasting states of the Early Triassic Earth system and divergent mechanisms for eventual restoration of oxic oceans and associated biotic recovery. Under the low-productivity scenario, climate warmth and reduced ocean circulation would have limited oxygen supply and recovery would reflect climate cooling and an associated enhancement of meridional circulation. Under the high-productivity scenario, enhanced nutrient delivery would have fueled primary production in excess of the oxygen available for respiration of that organic matter; recovery would reflect reduced nutrient availability, productivity, and associated oxygen demand.

Comparison of carbon isotope ($\delta^{13}C$) values along a depth gradient in Lower Triassic rocks provides a test between the low- and high-

* Corresponding author.
E-mail address: meyerk@stanford.edu (K.M. Meyer).

0012-821X/$ – see front matter © 2010 Elsevier B.V. All rights reserved.
doi:10.1016/j.epsl.2010.12.033

productivity scenarios. In the modern ocean, the transport of nutrients and organic matter from surface waters to the deep ocean, the "biological pump," causes a vertical separation of surface water carbon fixation from the deeper water remineralization. The kinetic isotopic effect associated with photosynthesis enriches the surface waters in ^{13}C of inorganic carbon and the remineralization of ^{13}C-depleted organic matter at depth maintains a $\delta^{13}C$ gradient of approximately 2‰ in dissolved inorganic carbon (DIC) today. If marine primary productivity was greatly reduced during Early Triassic time, the $\delta^{13}C_{DIC}$ gradient from shallow to deep water would have been smaller than present. Conversely, if productivity was elevated, the vertical gradient in the $\delta^{13}C$ of dissolved inorganic carbon ($\delta^{13}C_{DIC}$) would have been larger (Hilting et al., 2008).

2. Field setting and methods

To examine the strength of the biological pump during recovery from mass extinction, we measured the $\delta^{13}C$ composition of limestone samples from the Great Bank of Guizhou (GBG), an exceptionally exposed carbonate platform in the Nanpanjiang Basin of south China. A syncline dissects the GBG, providing a cross-sectional exposure of thick Upper Permian through Middle Triassic stratigraphic sections along a paleobathymetric gradient from the shallow-water (intertidal to tens of meters) platform interior to deep-water (hundreds of meters) basin margin environments (Fig. 1) (Lehrmann et al., 1998). Sections are correlated based upon physical stratigraphic relations and conodont and foraminiferan biostratigraphy (Lehrmann et al., 1998; Payne et al., 2004).

Geochemical and stable isotopic analyses were performed in the Stanford University Stable Isotopic Laboratory. Limestone samples were powdered using a 0.8 mm dental drill bit. Micrites were selectively sampled, and calcite veins and fossils were avoided. Dolomitized intervals of Laolaicao and Dajiang were also sampled, but at a lower density, for completeness. For $\delta^{13}C$ and $\delta^{18}O$ analysis, 60–100 μg of dried powder was added to a glass reaction vial. Samples were individually acidified with H_3PO_4 at 70 °C for 600 s and analyzed using a Finnigan Kiel III carbonate device coupled to a MAT 252 isotope ratio mass spectrometer. Isotopic composition is reported in standard delta notation relative to the VPDB standard. Analytical precision was better than 0.055‰ for oxygen and 0.035‰ for carbon based on replicate measurements of a laboratory standard. For trace metal analysis, ~2 mg of dried, powdered limestone was dissolved in 1 M acetic acid. After centrifugation, the supernatant was removed and subjected to trace metal analysis (Mn, Sr) as well as Ca and Mg analysis using a TJA IRIS Advantage/1000 Radial ICAP Spectrometer with a solid state CID detector. Analytical precision was better than 5%. Weight percent $CaCO_3$ was determined using a UIC Model 5011 CO_2 Coulometer and a UIC Model 5030 acidification module; analytical precision was better than 1%.

3. Results

The Lower Triassic $\delta^{13}C$ records of all five stratigraphic sections presented in Fig. 2 show multiple carbon isotope shifts of up to 8‰ occur across the Permian–Triassic (P–T) boundary and extend into the Lower Triassic. The pattern and magnitude of $\delta^{13}C$ variation is consistent with previous findings on the GBG and

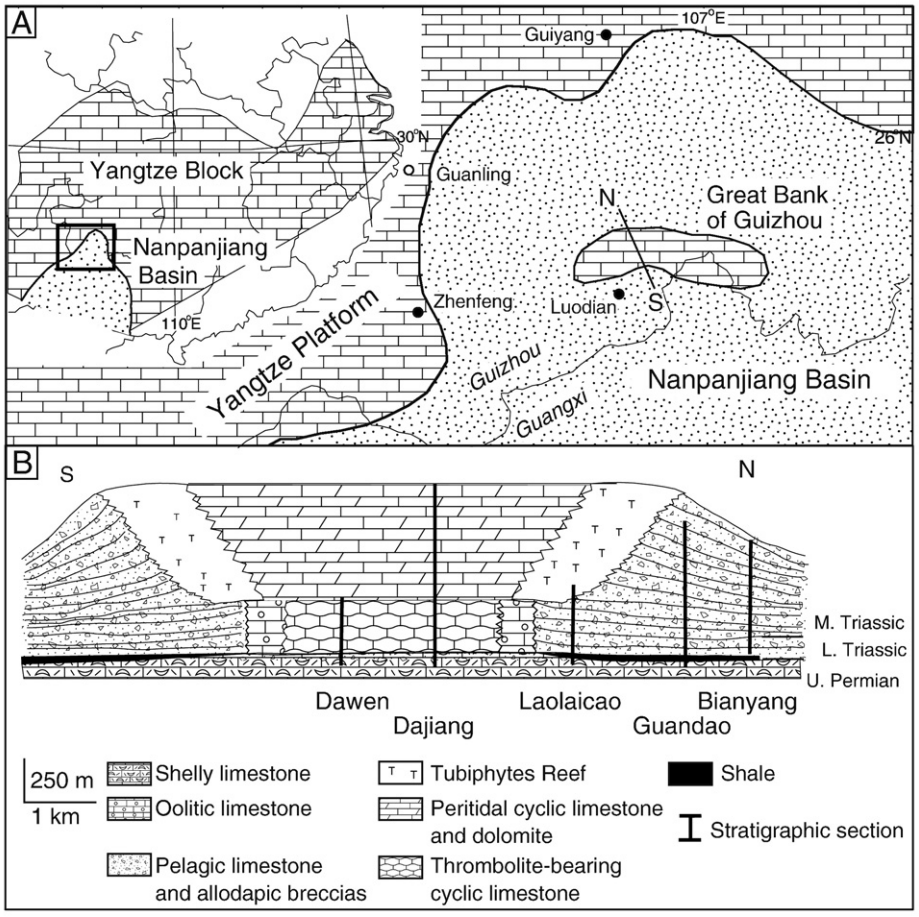

Fig. 1. (A) Paleogeographic map of the Early Triassic GBG, modified after (2). Inset: The stippled pattern indicates the Nanpanjiang Basin and the brick pattern represents the Yangtze Block. (B) Schematic cross section of the GBG, modified after (Payne et al., 2004). The vertical bars illustrate the locations of the stratigraphic sections within the GBG.

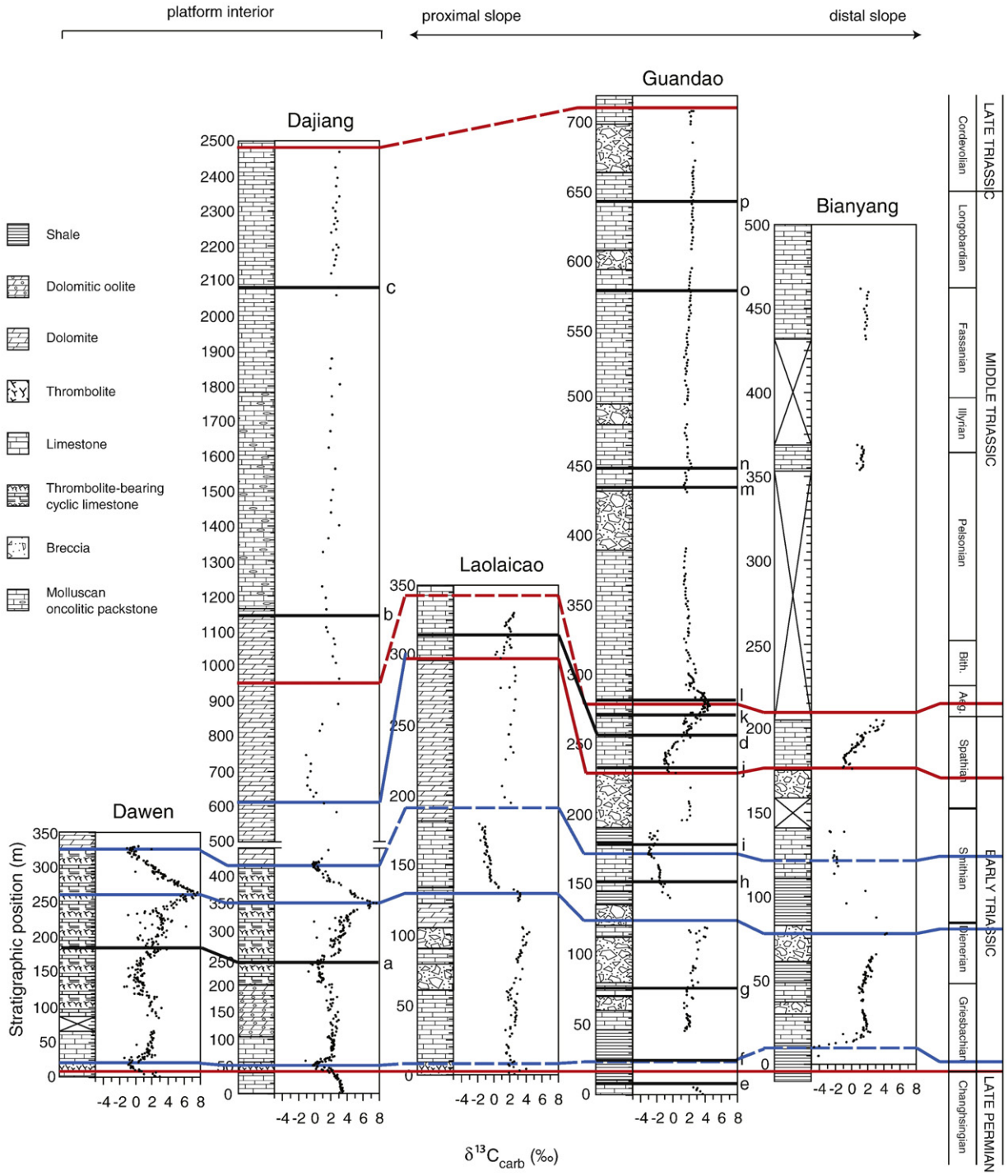

Fig. 2. Carbon isotopic data from all stratigraphic sections across the GBG. The time scale is based on conodont biostratigraphy from Guandao (*2*), and correlations are suggested based upon lithostratigraphic relationships (red) and carbon isotope trends (blue). Foraminifer (a–d) and conodont (e–p) first occurrences (except where noted): a. LAD *Rectocorniospira kalhori*, b. *Pilammina densa* and *Meandrospira dinarica*, c. *Aulotortus praegaschei*, d. *Endotriadella wirzi*, e. *Neogondolella changxingensis*, f. *Hindeodus parvus*, g. *Neospathodus dieneri*, h. *Ns. waageni*, i. *Ns. bansoni*, j. *Ns. honeri/symmetricus*, k. *Chiosella timorensis*, l. *Nicoraella germanicus/kockeli*, m. *Paragondolella bulgarica*, n. *Ng. constricta*, o. *Budurovignathus mungeonsis,* and p. *Metapolygnathus polygnathiformis.*

elsewhere in the Paleo-Tethys and Panthalassic Oceans (Atudorei, 1999; Horacek et al., 2007a,b, 2009; Payne et al., 2004; Richoz, 2004; Tong et al., 2007), indicating that they result from global secular variations in the isotope composition of the exogenic carbon reservoir. The $\delta^{13}C$ records stabilize near values of +2‰ during the Middle Triassic in platform interior and basin-margin sections (Fig. 2).

Lower Triassic $\delta^{13}C$ values are systematically enriched in the platform interior samples relative to the coeval slope and basin margin deposits by 2–4‰ at the peaks of correlative positive and negative $\delta^{13}C$ excursions during the Griesbachian, Dienerian, and Smithian substages (Fig. 3a). The difference in $\delta^{13}C$ between coeval deposits across the GBG decreases in the Spathian, and post-Bithynian Middle Triassic platform interior strata is nearly indistinguishable in

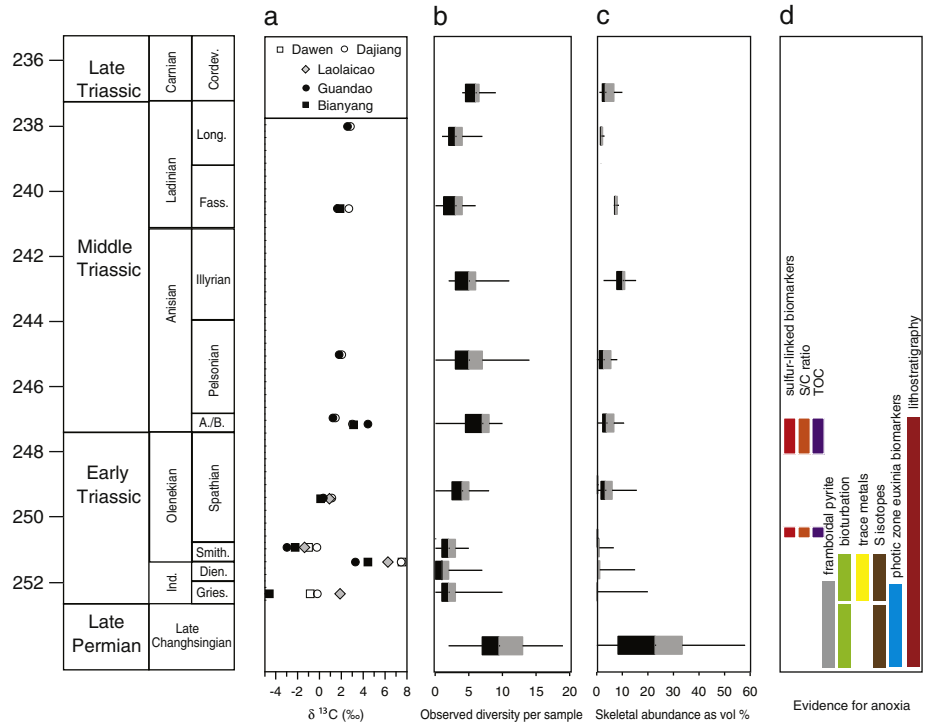

Fig. 3. (a) The Early and Middle $\delta^{13}C$ gradient across the GBG. Griesbachian to Smithian platform limestones are systematically enriched by 2–4‰ relative to coeval slope and basin strata. The $\delta^{13}C$ gradient decreases in the Smithian, and in the Middle Triassic, platform and basinal $\delta^{13}C$ values are nearly identical. (b and c) Box plots of diversity and fossil abundance observed on the GBG from the Late Permian into the Late Triassic. Data from (Payne et al., 2006). (d) Vertical bars show the temporal extent of anoxic or euxinic waters during the Late Permian and Early Triassic. Evidence is based on sulfur-linked biomarkers (red, (Takahashi et al., 2009)), S/C relationships (orange, (Takahashi et al., 2009)), total organic carbon (purple, (Takahashi et al., 2009)), bioturbation (green, (Kakuwa, 2008)), framboidal pyrite distributions (grey, (Nielsen and Shen, 2004; Twitchett and Wignall, 1996)), trace metal relationships (yellow, (Kakuwa, 2008)), sulfur isotopes (brown, (Newton et al., 2004; Nielsen and Shen, 2004)), lithostratigraphy (maroon, (Isozaki, 1997)), and biomarkers for photic zone euxinia (blue, (Grice et al., 2005)).

$\delta^{13}C$ composition from coeval beds on the basin-margin (Fig. 3a). Thus, the Lower Triassic interval of large $\delta^{13}C$ excursions is also characterized by a steep platform-to-basin gradient in $\delta^{13}C$, whereas the post-Bithynian interval of carbon isotope stability is characterized by little if any carbon isotope gradient from platform to basin. The magnitude of the isotope gradient is stable through the first half of the Lower Triassic, assuming a time-equivalence of the local maxima and minima in the $\delta^{13}C$ records across sections. Because similar isotope excursions occur in sections spanning Tethys and Panthalassa (Baud et al., 1996; Horacek et al., 2007a,b, 2009), we interpret the minima and maxima as time-correlative across sections. Any offset in the timing of isotope excursions among our sections (within biostratigraphic and lithostratigraphic constraints) would imply a large but fluctuating isotope gradient during Early Triassic time; no biostratigraphically permissible correlation scheme can remove the isotope gradient because the heaviest $\delta^{13}C$ values from the platform interior are several permil greater than those from the basin margin, and the lightest $\delta^{13}C$ values from the basin margin are several permil lighter than those from the platform interior. The near absence of an isotope gradient during the Middle Triassic is also insensitive to variation in stratigraphic correlation within available biostratigraphic constraints.

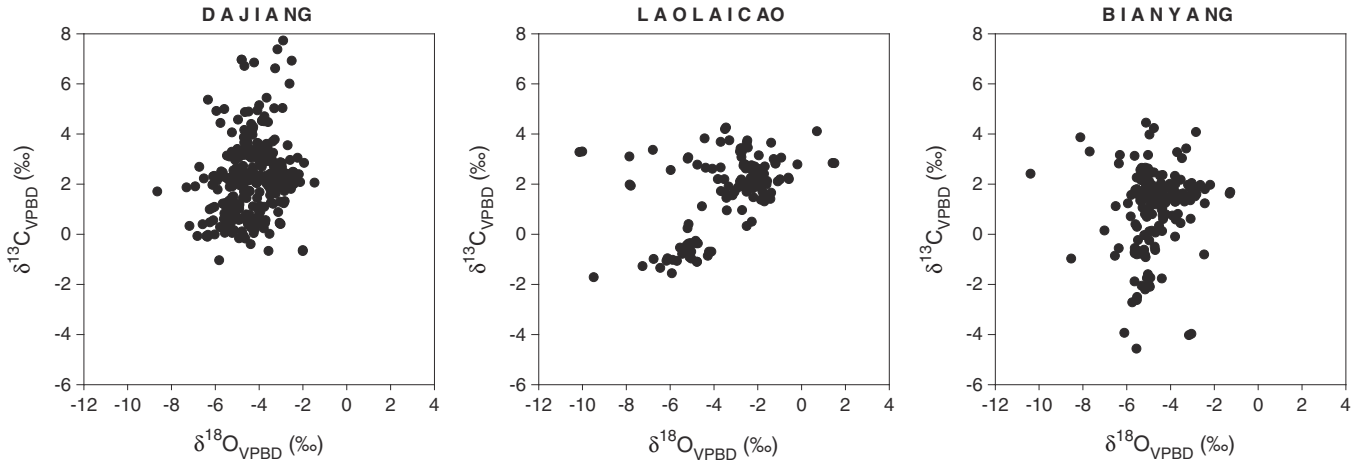

Fig. 4. Relationship between $\delta^{13}C$ and $\delta^{18}O$ for Dajiang, Laolaicao, and Bianyang limestones. The coefficients of determination (R^2) for linear regressions through these data are 0.04, 0.22, and 0.02, respectively.

4. Discussion

The results presented in Fig. 2 are consistent with the high-productivity scenario for the Early Triassic oceans with the isotope gradient reflecting differing $\delta^{13}C$ composition of shallow and deep waters during cementation; they are not predicted under the low-productivity scenario. The observed $\delta^{13}C$ gradient across the GBG could, in principle, also result from other processes: changes in the mixing ratio of sediment sources and minerals (aragonite versus calcite) with differing isotope compositions across the platform; preferential meteoric diagenesis of shallow-water strata; or greater diagenetic remineralization of organic carbon in deep-water settings. Detailed consideration of these alternatives shows that none can fully account for the observations.

Carbon isotopes are fractionated differently relative to seawater during aragonite versus calcite precipitation, so environmental and stratigraphic variation in carbonate mineralogy can produce $\delta^{13}C$ variability within and among facies and stratigraphic sections (Reuning et al., 2005; Swart and Eberli, 2005). However, the ~2‰ depletion of calcite relative to aragonite precipitated from the same water (Romanek et al., 1992) is too small to account for the differences in $\delta^{13}C$ between the platform interior and slope or the secular trends in $\delta^{13}C$ within stratigraphic sections. Moreover, nearly all carbonate sediment production probably occurred on the platform top. This view is supported by the general lack of carbonate-secreting plankton in the Triassic and the observation that slope sections contain abundant calciturbidites bearing skeletal and non-skeletal grains derived from shallow water environments (Lehrmann et al., 1998). Thus, changes in the proportional contribution of aragonite versus calcite to the platform sediments are unable to account for the extent of spatial and temporal variability in $\delta^{13}C$.

Subaerial exposure and meteoric diagenesis could provide a source of isotopically depleted carbon and oxygen that would exchange with C and O in carbonate sediments. This process would lead to depleted $\delta^{13}C$ and $\delta^{18}O$ in the platform interior relative to deeper water

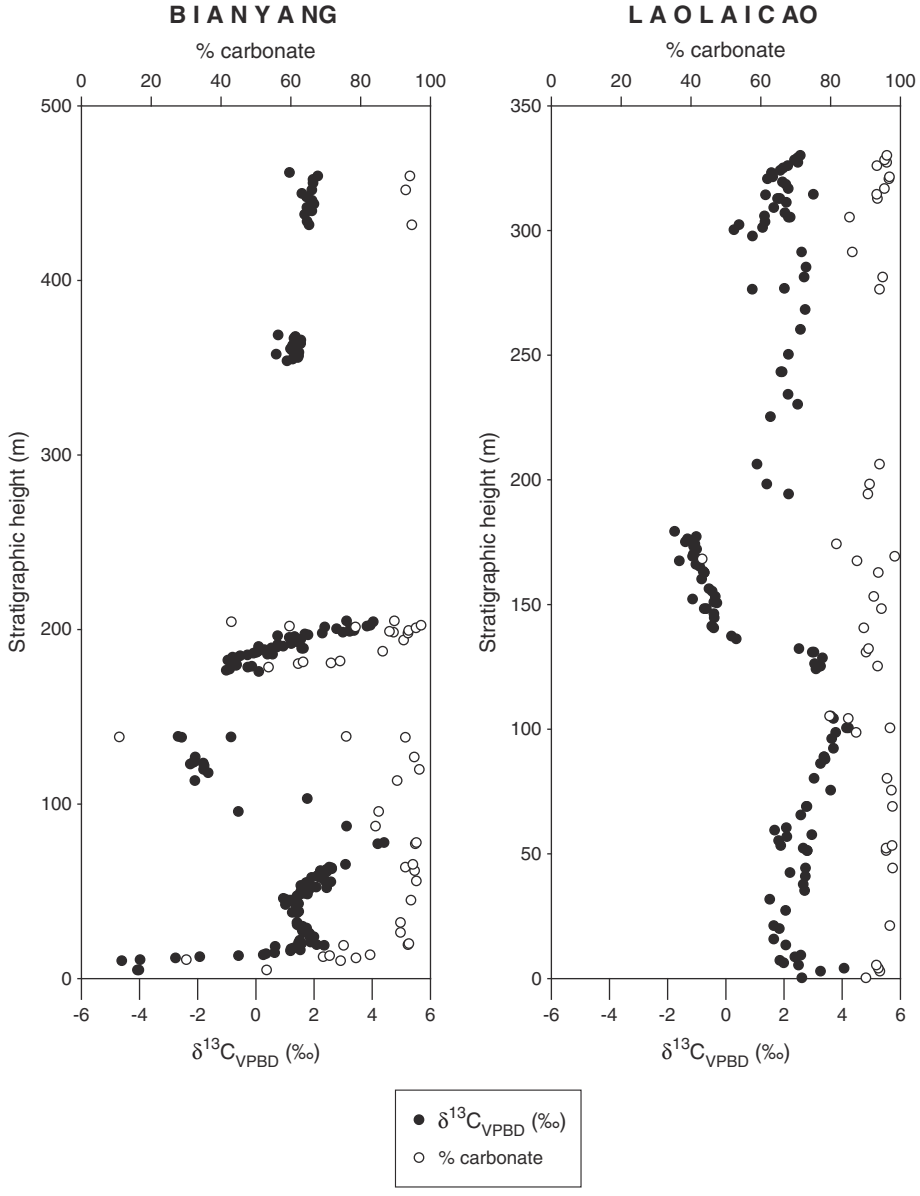

Fig. 5. Carbonate content (filled circles) and $\delta^{13}C$ (open circles) plotted against stratigraphic height for the Bianyang and Laolaicao localities. With the exception of the base of Bianyang, percent carbonate and $\delta^{13}C$ do not co-vary.

sections (Immenhauser et al., 2002; Knauth and Kennedy, 2009), a pattern opposite in sense to that observed on the GBG. Further, oxygen and carbon isotope values on the GBG do not exhibit the positive correlation predicted to accompany a significant meteoric alteration (Fig. 4; Knauth and Kennedy, 2009).

Because organic carbon is ^{13}C-depleted relative to normal marine DIC (generally near−30‰), precipitation of carbonate cements derived from remineralized organic carbon in porewaters during early diagenesis can decrease the $\delta^{13}C$ of limestone. Thus, higher initial organic carbon content or more efficient respiration of organic matter within basinal sediments could produce a gradient in $\delta^{13}C$. Triassic strata on the GBG have very high percent carbonate (Fig. 5), so the amount of organic matter-derived carbonate that would be required to produce the gradient is large. Given the measured platform $\delta^{13}C$ values and an observed 4‰ gradient, 20% of the slope carbonate would have to be derived from organic carbon remineralized within the sediment to be responsible for the observed gradient. Low TOC in Triassic strata from the platform top (<0.2% TOC; Krull et al., 2004) indicates that sufficient organic carbon to drive such a shift was unavailable on the platform top. Such a large contribution of organic-derived carbonate cannot be completely ruled out for the slope strata. However, it would be unlikely if the GBG sediments on the platform top and slope were similar to their counterparts on modern carbonate platforms, which generally contain little organic matter (Schwarz and Rendle-Buhring, 2005). Remineralization of organic matter within the slope sediments could more easily account for the observed gradient in the (~5) samples with the most negative $\delta^{13}C$ values at the base of the Bianyang section, because these lower-carbonate samples would have required less respired organic matter to produce depleted $\delta^{13}C$ values. Alternatively, authigenic methane production in platform interior sediments could elevate $\delta^{13}C$ relative to basinal limestones; the incorporation of oxidized methane into carbonate cements would reduce $\delta^{13}C$ values. However, because methanogenesis and methane oxidation are predicted to be spatially variable, the data do not support this possibility.

We prefer to interpret the more depleted $\delta^{13}C$ values toward the basin as reflecting DIC input from ^{13}C-depleted deep waters during early diagenesis in a highly productive ocean for three reasons: 1) differences in isotope composition during initial sediment production appear unlikely because the bulk of the carbonate sediment on the slope was produced on the platform and subsequently transported to deeper water; 2) the alternatives discussed above fail to account for the magnitude and direction of the Lower Triassic isotope gradient; and 3) alternative scenarios also fail to explain why the collapse of the isotope gradient coincides with carbon cycle stabilization and accelerated biotic recovery in the GBG (Fig. 3b and c). Under the high productivity scenario, the collapse of the isotope gradient is predicted to mark a reduction in productivity levels and an associated transition back to an oxygenated, lower-nutrient ocean, explaining the isotope gradient's association with biotic recovery. As hypothesized, global evidence for anoxia wanes in the Middle Triassic (Fig. 3d), and is coeval with GBG carbon cycle stabilization and biotic recovery.

Biogeochemical modeling provides a quantitative framework for understanding the relationships between primary productivity, ocean redox, and $\delta^{13}C$ during the Permian and Triassic. Using an Earth system model of intermediate complexity configured to end-Permian conditions, Meyer et al. (2008) explored controls on marine euxinia by varying the phosphate content of the ocean. The focus of the study was on phosphate and sulfur biogeochemistry, but the model also generated $\delta^{13}C_{DIC}$ results. Fig. 6 reports the model-generated vertical $\delta^{13}C_{DIC}$, O_2, and H_2S gradients at modern and 10x modern phosphate levels. As oceanic phosphate increases in the simulations, primary and export productivity increase and the vertical $\delta^{13}C_{DIC}$ gradient expands. At the same time, enhanced oxygen demand promotes

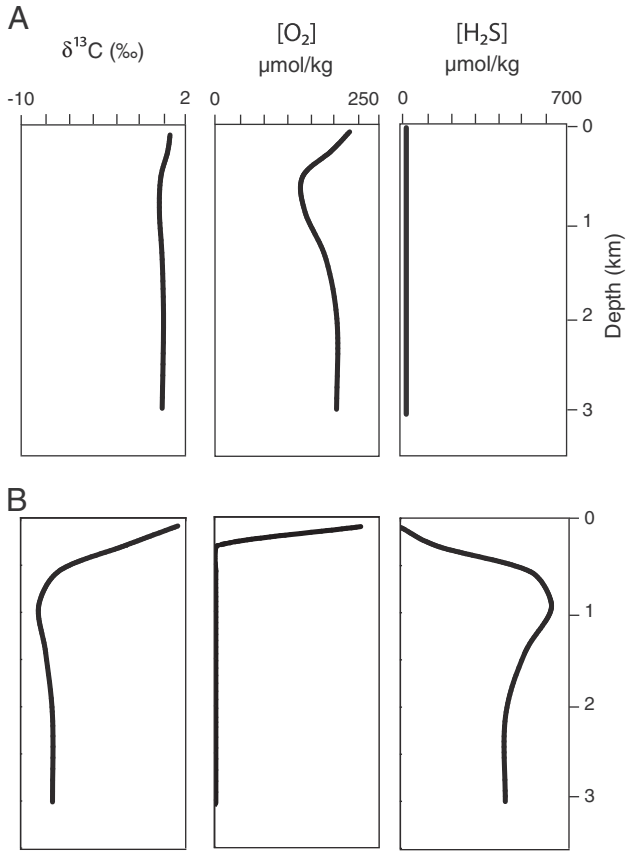

Fig. 6. (A) Modeled vertical $\delta^{13}C$, $[O_2]$, and $[H_2S]$ profiles from the Panthalassic Ocean in an ocean with modern phosphate content. (B) Modeled $\delta^{13}C$, $[O_2]$, and $[H_2S]$ profiles from the Panthalassic Ocean in an ocean with ten times the modern phosphate content.

anoxic and sulfidic conditions at depth. A tripling of the modern phosphate reservoir is required to produce $[H_2S]$ that is spatially consistent with geological data and a vertical $\delta^{13}C_{DIC}$ gradient of 4‰, the minimum needed to account for our observations. A higher phosphate concentration and consequently larger isotope gradient are more likely, given the incomplete exchange of carbonate carbon during cementation. Low productivity (i.e., low nutrient) scenarios fail to reproduce the observed $\delta^{13}C$ gradient in the marine water column.

There are few direct constraints on Early and Middle Triassic rates of primary production elsewhere, but whatever evidence exists suggests high productivity was not limited to the Nanpanjiang Basin. Molecular and isotopic data from Meishan and Spitsbergen support the notion of high productivity at the P–T boundary globally (Grice et al., 2005; Nabbefeld et al., 2010). Widespread geochemical and sedimentary evidence for anoxia (Fig. 3) and the occurrence of biomarkers for anoxygenic phototrophic bacteria throughout the Lower Triassic on the GBG and elsewhere (Hays, 2010) indicate the global persistence of biogeochemical conditions similar to those observed in the Nanpanjiang Basin throughout Early Triassic time.

5. Conclusions

Siberian trap volcanism and associated contact metamorphism of carbon-rich sedimentary strata provide a plausible control on the extent and timing of Early Triassic anoxia and euxinia. These events coincided with the end-Permian mass extinction and may have continued through part or all of Early Triassic time (Reichow et al., 2009), releasing as much as 100,000 Gt C into the atmosphere (Svensen et al., 2009), perhaps episodically (Payne and Kump, 2007).

Volatile release and consequent climate warming would have caused an intensification of the hydrological cycle, increased continental weathering, and thus additional nutrient (phosphate) delivery to the oceans, consistent with the large positive excursion in $^{87}Sr/^{86}Sr$ during the Early Triassic (Korte et al., 2006). Phosphate liberation from sediments under anoxic conditions would have functioned as a positive feedback serving to further elevate productivity and sustain euxinia (Payne and Kump, 2007; Payne and van de Schootbrugge, 2007; Van Cappellen and Ingall, 1994). Waning of volcanism, associated volatile release, and consequent silicate weathering would have reduced the phosphate delivery flux to the oceans, eventually causing phosphate levels to decline and reducing the extent of anoxia.

If the temporal correspondence between a large $\delta^{13}C$ gradient and delayed recovery from the end-Permian mass extinction reflects a causal connection, then the poverty of the Early Triassic fossil record may be a consequence of too much productivity rather than too little.

Supplementary data associated with this article can be found, in the online version, at doi:10.1016/j.epsl.2010.12.033.

Acknowledgements

The authors thank E. Schaal, X. Li, and H. Fu for assistance in the field; D. Mucciarone and G. Li for laboratory assistance; members of the Stanford Paleobiology lab for discussion; and J. Ingle, L. Kump, A. Turchyn, and B. van de Schootbrugge for constructive feedback on the manuscript. Meyer acknowledges support from the Agouron Institute. This work was supported by NSF grant EAR-0807377-007, ACS PRF grant 45329-G8, and NGS grant 8102-06.

References

Atudorei, N.-V., 1999. Constraints on the Upper Permian to Upper Triassic marine carbon isotope curve. Case studies from the Tethys. University of Lausanne.
Baud, A., Atudorei, V., Sharp, Z., 1996. Late Permian and early Triassic evolution of the Northern Indian margin: carbon isotope and sequence stratigraphy. Geodin. Acta 9, 57–77.
Erwin, D.H., 2006. Extinction: how life on earth nearly ended 250 million years ago. Princeton University Press, Princeton, N.J.. 296 pp.
Erwin, D.H., 2007. Disparity: morphological pattern and developmental context. Palaeontology 50, 57–73.
Flugel, E., 2002. Triassic reef patterns. In: Kiessling, W., Flugel, E., Golonka, J. (Eds.), Phanerozoic reef patterms: SEPM (Society for Sedimentary Geology) Special Publication, vol. 72, pp. 735–744.
Grice, K., Cao, C.Q., Love, G.D., Bottcher, M.E., Twitchett, R.J., Grosjean, E., Summons, R.E., Turgeon, S.C., Dunning, W., Jin, Y.G., 2005. Photic zone euxinia during the Permian–Triassic superanoxic event. Science 307, 706–709.
Hallam, A., 1991. Why was there a delayed radiation after the end-Paleozoic extinction? Hist. Biol. 5, 257–262.
Hays, L.E., 2010. Biogeochemical proxies for environmental and biotic conditions at the Permian-Triassic boundary. Massachusetts Institute of Technology.
Hilting, A.K., Kump, L.R., Bralower, T.J., 2008. Variations in the oceanic vertical carbon isotope gradient and their implications for the Paleocene–Eocene biological pump. Paleoceanography 23.
Horacek, M., Brandner, R., Abart, R., 2007a. Carbon isotope record of the P/T boundary and the Lower Triassic in the Southern Alps: evidence for rapid changes in storage of organic carbon. Palaeogeogr. Palaeoclimatol. Palaeoecol. 252, 347–354.
Horacek, M., Richoz, S., Brandner, R., Krystyn, L., Spötl, C., 2007b. Evidence for recurrent changes in Lower Triassic oceanic circulation of the Tethys: the $\delta^{13}C$ record from marine sections in Iran. Palaeogeogr. Palaeoclimatol. Palaeoecol. 252, 355–369.
Horacek, M., Koike, T., Richoz, S., 2009. Lower Triassic $\delta^{13}C$ isotope curve from shallow-marine carbonates in Japan, Panthalassa realm: confirmation of the Tethys $\delta^{13}C$ curve. J. Asian Earth Sci. 36, 481–490.
Hotinski, R.M., Bice, K.L., Kump, L.R., Najjar, R.G., Arthur, M.A., 2001. Ocean stagnation and end-Permian anoxia. Geology 29, 7–10.
Immenhauser, A., Kenter, J.A.M., Ganssen, G., Bahamonde, J.R., Van Vliet, A., Saher, M.H., 2002. Origin and significance of isotope shifts in Pennsylvanian carbonates (Asturias, NW Spain). J. Sed. Res. 72, 82–94.
Isozaki, Y., 1997. Permo–Triassic boundary superanoxia and stratified superocean: records from lost deep sea. Science 276, 235–238.
Kakuwa, Y., 2008. Evaluation of palaeo-oxygenation of the ocean bottom across the Permian–Triassic boundary. Glob. Planet. Change 63, 40–56.
Knauth, L.P., Kennedy, M.J., 2009. The late Precambrian greening of the Earth. Nature 460, 728–732.
Korte, C., Jasper, T., Kozur, H.W., Veizer, J., 2006. Sr-87/Sr-86 record of Permian seawater. Palaeogeogr. Palaeoclimatol. Palaeoecol. 240, 89–107.
Krull, E.S., Lehrmann, D.J., Druke, D., Kessel, B., Yu, Y.Y., Li, R.X., 2004. Stable carbon isotope stratigraphy across the Permian-Triassic boundary in shallow marine carbonate platforms, Nanpanjiang Basin, south China. Palaeogeogr. Palaeoclimatol. Palaeoecol. 204, 297–315.
Lehrmann, D.J., Wei, J.Y., Enos, P., 1998. Controls on facies architecture of a large Triassic carbonate platform: the Great Bank of Guizhou, Nanpanjiang Basin, South China. J. Sed. Res. 68, 311–326.
Meyer, K.M., Ridgwell, A., Kump, L.R., 2008. Biogeochemical controls on photic zone euxinia during the end-Permian mass extinction. Geology 36, 747–750.
Nabbefeld, B., Grice, K., Twitchett, R.J., Summons, R.E., Hays, L., Böttcher, M.E., Muhammad, A., 2010. An integrated biomarker, isotopic and palaeoenvironmental study through the Late Permian event at Lusitaniadalen, Spitsbergen. Earth Planet. Sci. Lett. 291, 84–96.
Newton, R.J., Pevitt, E.L., Wignall, P.B., Bottrell, S.H., 2004. Large shifts in the isotopic composition of seawater sulphate across the Permo–Triassic boundary in northern Italy. Earth Planet. Sci. Lett. 218, 331–345.
Nielsen, J.K., Shen, Y., 2004. Evidence for sulfidic deep water during the Late Permian in the East Greenland Basin. Geology 32, 1037–1040.
Payne, J.L., Finnegan, S., 2006. Controls on marine animal biomass through geological time. Geobiology 4, 1–10.
Payne, J.L., van de Schootbrugge, B., 2007. Life in Triassic Oceans: links between planktonic and benthic recovery and radiation. In: Falkowski, P.G., Knoll, A.H. (Eds.), Evolution of Primary Producers in the Sea. Academic Press, Amsterdam, pp. 165–189.
Payne, J.L., Lehrmann, D.J., Wei, J.Y., Orchard, M.J., Schrag, D.P., Knoll, A.H., 2004. Large perturbations of the carbon cycle during recovery from the end-Permian extinction. Science 305, 506–509.
Payne, J.L., Lehrmann, D.J., Wei, J.Y., Knoll, A.H., 2006. The pattern and timing of biotic recovery from the end-Permian extinction on the Great Bank of Guizhou, Guizhou province, China. Palaios 21, 63–85.
Rampino, M.R., Caldeira, K., 2005. Major perturbation of ocean chemistry and a 'Strangelove Ocean' after the end-Permian mass extinction. Terra Nova 17, 554–559.
Payne, J.L., Kump, L.R., 2007. Evidence for recurrent Early Triassic massive volcanism from quantitative interpretation of carbon isotope fluctuations. Earth Planet. Sci. Lett. 256, 264–277.
Reichow, M.K., Pringle, M.S., Al'mukhamedov, A.I., Allen, M.B., Andreichev, V.L., Buslov, M.M., Davies, C.E., Fedoseev, G.S., Fitton, J.G., Inger, S., Medvedev, A.Y., Mitchell, C., Puchkov, V.N., Safonova, I.Y., Scott, R.A., Saunders, A.D., 2009. The timing and extent of the eruption of the Siberian Traps large igneous province: implications for the end-Permian environmental crisis. Earth Planet. Sci. Lett. 277, 9–20.
Reuning, L., Reijmer, J.J.G., Betzler, C., Swart, P., Bauch, T., 2005. The use of paleoceanographic proxies in carbonate periplatform settings—opportunities and pitfalls. Sed. Geol. 175, 131–152.
Richoz, S., 2004. Stratigraphy and carbon isotope study of the Upper Permian and Lower Triassic in some localities of the Neotethyan realm (Turkey, Oman, Iran). University of Lausanne.
Romanek, C.S., Grossman, E.L., Morse, J.W., 1992. Carbon isotopic fractionation in synthetic aragonite and calcite—effects of temperature and precipitation rate. Geochim. Cosmochim. Acta 56, 419–430.
Schwarz, J., Rendle-Buhring, R., 2005. Controls on modern carbonate preservation in the southern Florida Straits. Sed. Geol. 175, 153–167.
Svensen, H., Planke, S., Polozov, A.G., Schmidbauer, N., Corfu, F., Podladchikov, Y.Y., Jamtveit, B., 2009. Siberian gas venting and the end-Permian environmental crisis. Earth Planet. Sci. Lett. 277, 490–500.
Swart, P.K., Eberli, G., 2005. The nature of the delta C-13 of periplatform sediments: implications for stratigraphy and the global carbon cycle. Sed. Geol. 175, 115–129.
Takahashi, S., Yamakita, S., Suzuki, N., Kaiho, K., Ehiro, M., 2009. High organic carbon content and a decrease in radiolarians at the end of the Permian in a newly discovered continuous pelagic section: a coincidence? Palaeogeogr. Palaeoclimatol. Palaeoecol. 271, 1–12.
Tong, J., Zuo, J., Chen, Z.Q., 2007. Early Triassic carbon isotope excursions from South China: proxies for devastation and restoration of marine ecosystems following the end-Permian mass extinction. Geol. J. 42, 371–389.
Twitchett, R.J., 2006. The palaeoclimatology, palaeoecology and palaeo environmental analysis of mass extinction events. Palaeogeogr. Palaeoclimatol. Palaeoecol. 232, 190–213.
Twitchett, R.J., Wignall, P.B., 1996. Trace fossils and the aftermath of the Permo–Triassic mass extinction: evidence from northern Italy. Palaeogeogr. Palaeoclimatol. Palaeoecol. 124, 137–151.
Twitchett, R.J., Looy, C.V., Morante, R., Visscher, H., Wignall, P.B., 2001. Rapid and synchronous collapse of marine and terrestrial ecosystems during the end-Permian biotic crisis. Geology 29, 351–354.
Van Cappellen, P., Ingall, E.D., 1994. Benthic phosphorus regeneration, net primary production, and ocean anoxia: a model of the coupled marine biogeochemical cycles of carbon and phosphorus. Paleoceanography 9, 677–692.
Wignall, P.B., Twitchett, R.J., 2002a. Extent, duration, and nature of the Permian–Triassic superanoxic event. In: Koeberl, C., MacLeod, K.C. (Eds.), Catastrophic Events and Mass Extinctions: Impacts and Beyond. : Geological Society of America Special Paper, 356. Boulder, Colorado, pp. 395–413.
Wignall, P.B., Twitchett, R.J., 2002b. Permian–Triassic sedimentology of Jameson Land, East Greenland: incised submarine channels in an anoxic basin. J. Geol. Soc. 159, 691–703.
Xie, S.C., Pancost, R.D., Yin, H.F., Wang, H.M., Evershed, R.P., 2005. Two episodes of microbial change coupled with Permo/Triassic faunal mass extinction. Nature 434, 494–497.